Optical Engineering

SPIEDigitalLibrary.org/oe

Focusing properties of elliptical mirror with an aperture angle greater than π

Jian Liu
Min Ai
He Zhang
Jiubin Tan

SPIE

Focusing properties of elliptical mirror with an aperture angle greater than π

Jian Liu
Min Ai
He Zhang
Jiubin Tan
Harbin Institute of Technology
Center of Ultra-Precision Optoelectronic Instrument Engineering
Harbin 150001, China
E-mail: jbtan@hit.edu.cn

Abstract. An analytical apodization function of an elliptical mirror with an aperture angle greater than π is derived for the analysis of the focusing properties. The distribution of electric field intensity near the focal region is given using vectorial Debye theory. Simulation results indicate that a bone-shaped focal spot is formed under linearly polarized illumination, and a tight-circularly symmetric spot is generated under radially polarized illumination. The change in eccentricity causes such a change in the focusing pattern under radially polarized illumination, that a greater eccentricity causes a spot tighter in transverse direction but wider in axial direction. Under radially polarized illumination, the transverse and axial full-width-at-half-maximum will be 0.382λ and 0.757λ, respectively, and the conversion efficiency of the longitudinal component can go beyond 99%, when the semi-aperture angle is $2\pi/3$ and the eccentricity is 0.6. It can, therefore, be concluded that the tight focusing pattern with strong and pure longitudinal field can be achieved under radially polarized illumination for particle acceleration, optical tweezers, and high-resolution scanning microscopy. [DOI: 10.1117/1.OE.53.6.061606]

Subject terms: elliptical mirror; apodization function; linear or radial polarization; conversion efficiency.

Paper 130915SS received Jul. 8, 2013; revised manuscript received Aug. 29, 2013; accepted for publication Sep. 4, 2013; published online Dec. 2, 2013.

1 Introduction

Elliptical mirror is an alternative focusing element which can be used as an objective lens during optical scanning microscopy or molecule imaging.[1–3] Although aberrations such as coma and astigmatism caused by the assembly errors and the poor off-axis properties of these mirrors have limited even the low-aperture applications of them in the past few decades,[4–7] with the fast development of precision engineering, they have been developed and produced for high-aperture angle applications. Aperture angle of an elliptical mirror in this article indicates the full-covering angle at the focal spot. An elliptical mirror is free from chromatic aberration, and it can enable aperture angle to reach π or even go beyond π,[2] which means tighter focal spots may be obtained. Compared with objective lenses, elliptical mirrors can be easily used for the extension of aperture angles. What is more, using elliptical mirrors with aperture angles greater than π, the specimen can be put in forward and backward illuminations. The focal spot of a focusing system with a high-aperture angle is always tight, and therefore, vectorial Debye theory and the apodization function are used to describe the focusing patterns of the elliptical mirrors.[1,8,9] Apodization function reveals the energy redistribution in the spherical wavefront on the exit pupil, while it is passing through or being reflected by a focusing element. The spherical wavefront can approximately be equal to the wavefront over the aperture of a focusing element, but this approximation is valid only in the low-aperture case. When the aperture angle is high, the difference between the spherical wavefront and the wavefront over the focusing element's aperture cannot be negligible. The energy distribution is totally different when it is being focused by a lens, a parabolic mirror, or an elliptical mirror in the high-aperture case. The focusing properties of a lens, a parabolic mirror, or an elliptical mirror with high-aperture angle, but less than π, have been discussed in Refs. 10, 7 and 8, and 1 and 3, respectively. An apodization function has been derived earlier in differential form for a focusing elliptical mirror, but it is not applicable for the analysis we intend to do in this article, because the aperture is now greater than π. The simulation based on that apodization function will also be time consuming, because the function is not analytic. Therefore, it is of great necessity to derive an analytic expression of apodization function before the focusing properties of an elliptical mirror with aperture greater than π can properly be analyzed.

2 Derivation of Apodization Function

Apodization function, $p(\theta)$, is defined as the ratio of exit amplitude to incident amplitude on a mirror at focusing angle θ; and if the energy loss caused by reflection or absorption can be negligible, it will be expressed as[1]

$$p(\theta) = \frac{a+c}{a-c}\sqrt{\frac{\sin\alpha d\alpha}{\sin\theta d\theta}}, \tag{1}$$

where α is the divergence angle at F_1 and θ is the convergence angle at F_2, as shown in Fig. 1. Points F_1 and F_2 are the two conjugate foci of the elliptical mirror in an elliptical mirror-based system (EMBS). The position of focus F_1 coincides with the focus of the lens. The plane wave converges to focus F_1 after it passes through the lens. Then, the divergent

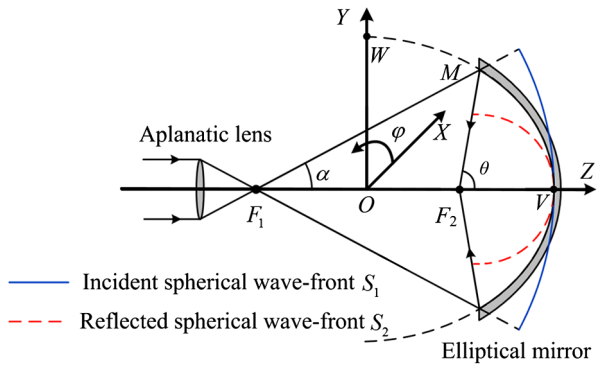

Fig. 1 Reflection on an elliptical mirror. $|OV| = a$, $|OW| = b$, and $|OF_1| = |OF_2| = c = \sqrt{a^2 - b^2}$. z' is the distance between M and F_2 along optical axis Z.

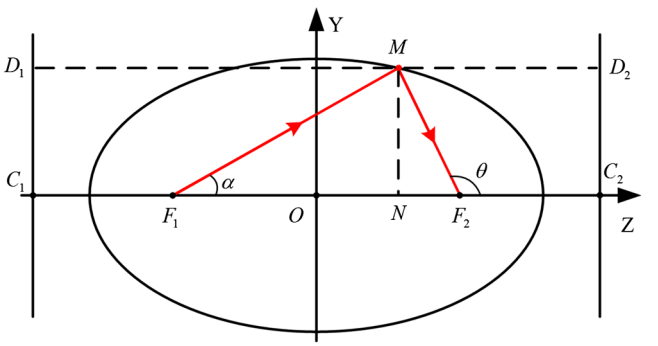

Fig. 2 Cross-section of ellipsoid in $Y - Z$ plane.

spherical wave propagates to the mirror surface. The wavefront before reflection is defined as S_1, and the wavefront after reflection is defined as S_2.

Further, as shown in Fig. 1, the mirror function is $z^2/a^2 + (x^2 + y^2)/b^2 = 1$, where $a = |OV|$ and $b = |OW|$ are the major and the minor semiaxes of the ellipse and $c = |OF_1| = |OF_2| = \sqrt{a^2 - b^2}$. The relationship between α and θ used to calculate $p(\theta)$ in Eq. (1) are shown below[1]

$$\alpha = \arctan[(z' - c)\tan\theta/(z' + c)], \tag{2}$$

$$z' = (ca^2\tan^2\theta + ab^2\sqrt{1 + \tan^2\theta})/(a^2\tan^2\theta + b^2), \quad (0 < \theta < \pi/2), \tag{3}$$

where z' is distance between M and F_2 along optical axis Z.

Equation (1) is derived from the definition of the apodization function, and it is valid no matter whether the semi-aperture angle θ is greater than $\pi/2$ or not. However, as Eqs. (2) and (3) are not continuous for $\theta = \pi/2$, Eqs. (1)–(3) cannot be used to describe the energy redistribution in the spherical wavefront on the exit pupil when the aperture angle (2θ) is greater than π. By introducing the eccentricity e of an ellipse, this difficulty can be overcome. Besides, the expression of the apodization function given in Eq. (1) is not analytic, and the simulation based on this expression will be limited to computation speed. An analytic expression of apodization function must be derived for the analysis of the focusing properties of an elliptical mirror with aperture angle greater than π.

The eccentricity e and the major semiaxis a are usually used to define an ellipsoid. e is equal to c/a, and the arbitrary ellipsoid value of e is a positive number less than 1. By substituting $e = \sqrt{a^2 - b^2}/a$ into the mirror function $z^2/a^2 + (x^2 + y^2)/b^2 = 1$,

$$\frac{x^2 + y^2}{a^2 - e^2a^2} = 1 - \frac{z^2}{a^2}. \tag{4}$$

As shown in Fig. 2, D_1C_1 and D_2C_2 are the directrixes of the ellipse, respectively. The eccentricity e is also equal to the ratio of the distance (such as the line MF_1) from any particular point on the ellipse to one of the foci at the perpendicular distance to the directrix from the same point (line MD_1), i.e., $e = MF_1/MD_1 = MF_2/MD_2$.

From the geometrical relationship in triangles F_1MN and F_2MN

$$\begin{aligned}\cos\alpha &= F_1N/F_1M = F_1N/eMD_1 \\ &= (z + c)/[e(z + a/e)] = (z + ea)/(a + ez),\end{aligned} \tag{5}$$

$$\begin{aligned}\cos\theta &= F_2N/F_2M = F_2N/eMD_2 = (z - c)/[e(a/e - z)] \\ &= (z - ea)/(a - ez).\end{aligned} \tag{6}$$

Angles α and θ can be expressed as shown below

$$\alpha = \arccos\left(\frac{z + ae}{a + ez}\right), \qquad \theta = \arccos\left(\frac{z - ae}{a - ez}\right). \tag{7}$$

Further,

$$\begin{aligned}\frac{d\alpha}{dz} &= -\frac{1}{\sqrt{1 - (z + ae)^2/(a + ez)^2}} \cdot \frac{a - ae^2}{(a + ae)^2}, \\ \frac{d\theta}{dz} &= -\frac{1}{\sqrt{1 - (z - ae)^2/(a - ez)^2}} \cdot \frac{a - ae^2}{(a - ae)^2}.\end{aligned} \tag{8}$$

By substituting Eqs. (7) and (8) into Eq. (1), the apodization function can be simplified as

$$\begin{aligned}p(\theta) &= \frac{a + ae}{a - ae}\sqrt{\frac{\sin\alpha d\alpha}{\sin\theta d\theta}} = \frac{1 + e}{1 - e}\sqrt{\frac{(a - ez)d\alpha}{(a + ez)d\theta}} \\ &= \frac{1 + e}{1 - e}\sqrt{\frac{(a - ez)d\alpha/dz}{(a + ez)d\theta/dz}} = \frac{1 + e}{1 - e} \cdot \frac{a - ez}{a + ez}.\end{aligned} \tag{9}$$

Equation (9) is the analytical expression of the apodization function for an elliptical mirror, and if θ_{max} is the largest semi-aperture angle of a given elliptical mirror, the apodization function will be continuous in domain of definition $[0, 2\theta_{max}]$, even $\theta_{max} \geq \pi/2$.

3 Focusing Patterns under Linearly Polarized Illumination

As shown in Fig. 3, the electric field of incident light wave is linearly polarized along the X-axis, and after it passes through the mirror and is reflected by the mirror, the electric field distribution near the focus F_2 can be described as shown below[1]

$$\begin{cases} \boldsymbol{E}_x = iA[I_0 + I_2 \cos(2\phi_s)], \\ \boldsymbol{E}_y = iAI_2 \sin(2\phi_s), \\ \boldsymbol{E}_z = -2AI_1 \cos \phi_s, \end{cases} \tag{10}$$

where A is a constant, which satisfies $A = \pi/\lambda$, and I_0, I_1, and I_2 are intermediate variables used to make the expressions of E_x, E_y, and E_z, respectively, compact, and they are expressed as shown below

$$\begin{cases} I_0 = \int_0^{\theta_{\max}} p(\theta) \sin\theta(1+\cos\theta) J_0(kr_s \sin\theta_s \sin\theta) e^{-ikr_s \cos\theta_s \cos\theta} \mathrm{d}\theta, \\ I_1 = \int_0^{\theta_{\max}} p(\theta) \sin^2\theta J_1(kr_s \sin\theta_s \sin\theta) e^{-ikr_s \cos\theta_s \cos\theta} \mathrm{d}\theta, \\ I_2 = \int_0^{\theta_{\max}} p(\theta) \sin\theta(1-\cos\theta) J_2(kr_s \sin\theta_s \sin\theta) e^{-ikr_s \cos\theta_s \cos\theta} \mathrm{d}\theta, \end{cases} \tag{11}$$

where $(r_s, \theta_s, \varphi_s)$ is spherical coordinates near the focus F_2, and J_n is a Bessel function of the first kind of order n.

The established expression of the electric field is used, and let the eccentricity e be 0.6, then the light field near the focus F_2 is acquired when the semi-aperture angle is $2\pi/3$. As shown in Fig. 4, the electric field intensity in the focal plane mainly consists of components which are polarized along the X- and Z-axes. The maximum values of field intensity in Figs. 4(a) and 4(c) are close to each other. The distribution of total intensity splits into two peaks, since the two main components are distributed in different directions. The bone-shaped distribution makes the focusing pattern different from the airy pattern in transverse direction, which is obtained using the low-aperture focusing lens.

The bone-shaped focusing pattern becomes more obvious as the aperture increases, which means the distance between two peaks further increases. This means that the depolarization effect becomes significant in the transverse direction under high-aperture conditions. Meanwhile, the component of the electric field along Z-axis is enhanced in intensity when the convergence angle increases.

It can be seen from Fig. 5 that the ratios of maximum intensity of component X to that of component Z versus the semi-aperture angle θ when $e = 0.6$ or $e = 0.8$ agree with each other, despite different eccentricities. It should be noted that, in the view of the fabrication technology, we only consider the semi-elliptical mirror. It means that the maximum semi-aperture angles $\theta_{\max}$ of elliptical mirrors

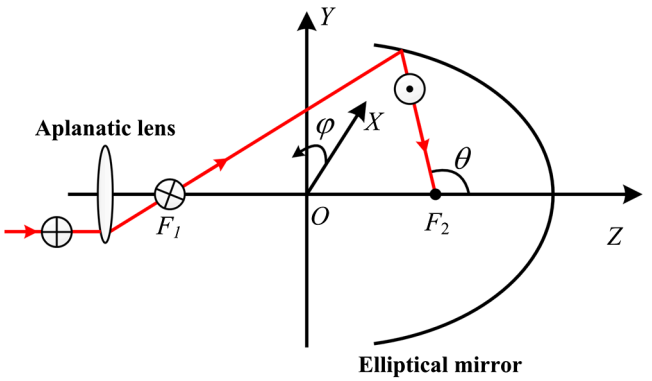

Fig. 3 Schematic diagram of focusing of an elliptical mirror. φ is the angle between the $X-Z$ plane and the meridian plane, and θ is the semi-aperture angle.

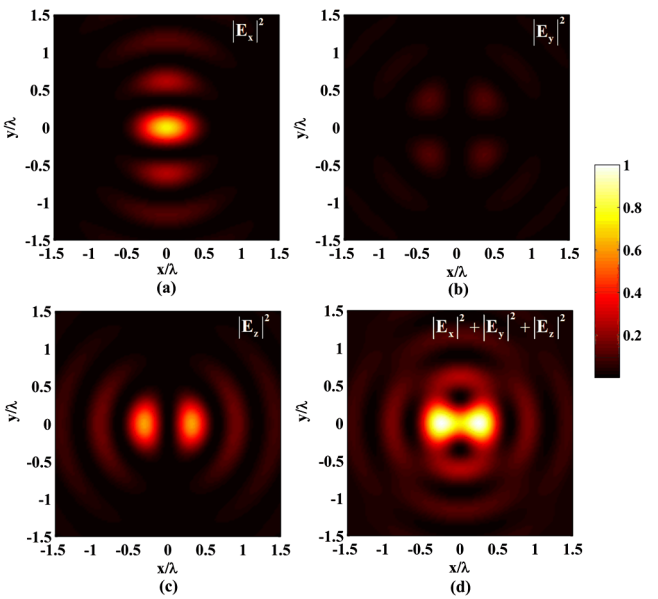

Fig. 4 Distribution of electric field intensity in the focal plane under linearly polarized illumination. (a)–(c) are intensity distributions of E_x, E_y and E_z; (d) is the total field intensity distribution.

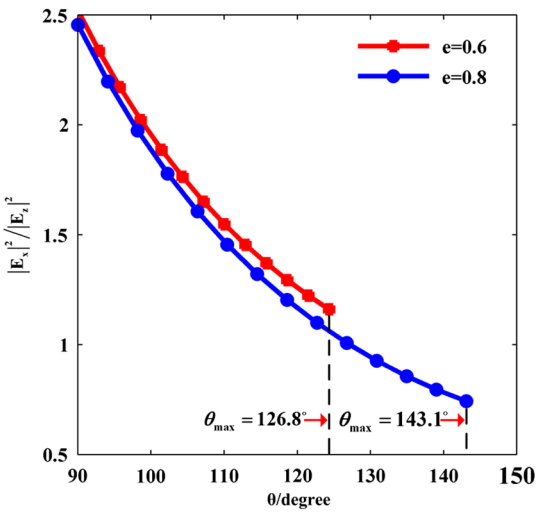

Fig. 5 Ratios of maximum intensity of component X to maximum intensity of component Z versus the semi-aperture angle θ.

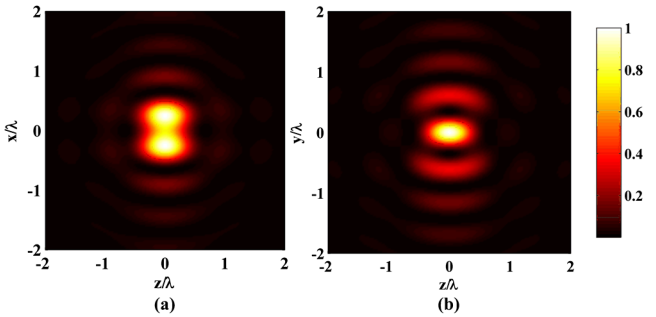

Fig. 6 Axial distribution of the electric field intensity under linearly polarized illumination. (a) and (b) are intensity distributions in the $X-Z$ and $Y-Z$ planes.

with different eccentricities are different, for example, when eccentricity e is 0.6, $\theta_{\max}=\pi-\arctan(4/3)$, which is slightly larger than 126 deg. Similarly, when e is 0.8, $\theta_{\max}$ is slightly larger than 143 deg. For an elliptical mirror with $e=0.8$, the electric field intensity of the component Z can be enhanced and finally exceeds the intensity of component X, as the angle θ increases. Theoretically, $\theta_{\max}$ could exceed 143 deg for a full elliptical mirror with $e=0.8$. In that case, the electric field intensity in the focal plane under linearly polarized illumination can still be calculated using Eqs. (9)–(11). However, the calculation is beyond the scope of this article, as such an elliptical mirror is difficult to fabricate.

Figure 6 shows the axial distribution of the electric field intensity, which is under the same condition as given in Fig. 4. It is clear that the spot will be compressed in the axial direction, as the semi-aperture angle increases.

4 Focusing Patterns under Radially Polarized Illumination

Since tight spots can be acquired under radially polarized illumination and the longitudinal component of the electric field near the focus is significant,[11–14] focusing properties of the elliptical mirrors under radially polarized illumination are discussed in the high-aperture case when the aperture angle is greater than π. The electric field near focus F_2 consists of radial and longitudinal components, and they can be expressed in cylindrical coordinates (ρ_s,θ_s,z_s), as shown below[3]

$$\begin{cases}\boldsymbol{E}_r(\rho_s,z_s)=A\int_0^{\theta_{\max}}\sin 2\theta p(\theta)l(\alpha)J_1(k\rho_s\sin\theta)e^{-ikz_s\cos\theta}\mathrm{d}\theta,\\ \boldsymbol{E}_z(\rho_s,z_s)=-2iA\int_0^{\theta_{\max}}\sin^2\theta p(\theta)l(\alpha)J_0(k\rho_s\sin\theta)e^{-ikz_s\cos\theta}\mathrm{d}\theta,\end{cases}\tag{12}$$

where $l(\alpha)$ describes a Bessel–Gauss beam waist at plane before the lens[15] and $l(\alpha)=\exp[-\beta^2(\sin\alpha/\mathrm{NA}_{\mathrm{LENS}})^2 J_1(2\beta_0\sin\alpha/\mathrm{NA}_{\mathrm{LENS}})]$. β is the ratio of the pupil radius to the beam waist before the aplanatic lens, which is set to be 1 in the general sense. The numerical aperture of the lens in the EMBS is 0.95. If eccentricity e is 0.6 and the semi-aperture angle is $2\pi/3$, the focal distributions of the light field will be as shown in Fig. 7. It is interesting to see that the distribution of the radial component is no longer a doughnut-shape, but it splits into two separate doughnut-shaped areas when the aperture angle is greater than π.

As shown in Fig. 8, the full-width-at-half-maximum (FWHM) of the point-spread function is nearly 0.38λ in the transverse direction and 0.76λ in the axial direction. The focal spot is tighter in size than the diffraction limit of a lens system, even when the numerical aperture of the lens is supposed to be 1.

The extent of compression for the focal spot benefits from a deep mirror, and so a deep elliptical mirror generates a spot

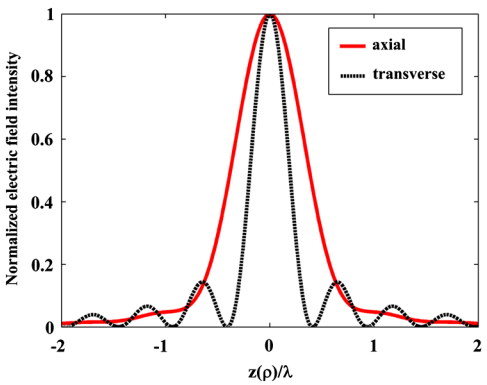

Fig. 8 Point-spread function of an elliptical mirror-based system (EMBS) with $e=0.6$, and $\theta_{\max}=2\pi/3$ in transverse and axial directions under radially polarized illumination.

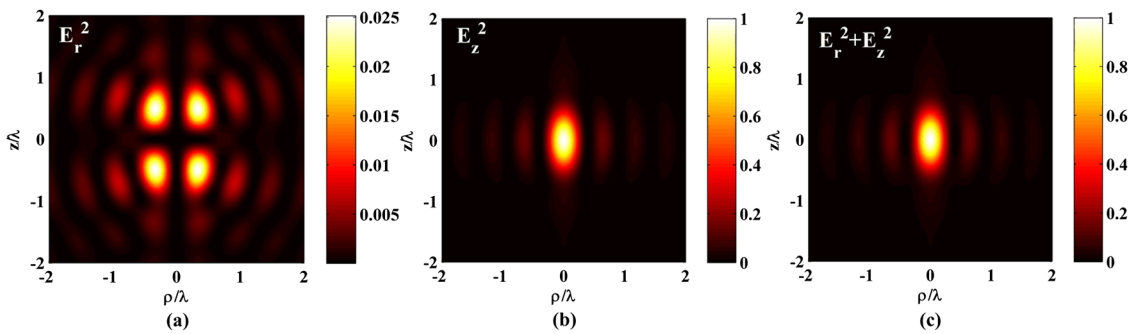

Fig. 7 Axial distribution of electric field intensity under radially polarized illumination. (a) and (b) are intensity distributions of E_r and E_z; (c) is the total field intensity distribution.

Table 1 Full-width-at-half-maximum (FWHM) in transverse and axial directions.

Semi-aperture angle (deg)	Transverse FWHM (λ)	Axial FWHM (λ)
	$e = 0.6$	
105	0.383	0.889
110	0.381	0.844
115	0.381	0.797
120	0.382	0.757
	$e = 0.8$	
105	0.377	0.945
110	0.376	0.894
115	0.378	0.851
120	0.383	0.815

tighter than that focused by a normal elliptical mirror. It can be seen from Table 1 that for a mirror with $e = 0.6$, the tightest spot in the transverse direction can be obtained when the semi-aperture angle is between 110 and 115 deg, and for a mirror with $e = 0.8$, the same thing can be obtained at nearly 110 deg. It is interesting to see that when compared with the variation tendency of transverse FWHM, axial FWHM decreases steadily as the aperture angle increases. Aperture extension causes the axial compression of the focal spot.

Another advantage of radially polarized illumination is that a high-longitudinal polarization conversion efficiency can be achieved in the focal plane,[13,16] and the efficiency can be defined as

$$\eta = \int_0^\infty |\boldsymbol{E}_z(\rho,0)|^2 2\pi\rho d\rho \Big/ \left(\int_0^\infty |\boldsymbol{E}_r(\rho,0)|^2 2\pi\rho d\rho + \int_0^\infty |\boldsymbol{E}_z(\rho,0)|^2 2\pi\rho d\rho \right). \quad (13)$$

Much work has been done on the realization of a strong longitudinally polarized focal field because of its applications such as particle acceleration, optical tweezers, and high-resolution microscopy. The existing lens systems can be used to increase the conversion efficiency to nearly 80%, which means that the energy of the longitudinal component within the focal volume is nearly four times stronger than that of the radial component. It can be seen from Fig. 9 that the biggest value of the ratios for different eccentricities are different, and the semi-aperture angles required to produce the tightest focal spot are not alike, too. A deeper elliptical mirror with $e = 0.8$ can focus a stronger longitudinal field than a shallower elliptical mirror with $e = 0.6$. The four lines in Fig. 9 reveal the maximum and the integral values of $|E_z|^2/|E_r|^2$ versus the semi-aperture angle, and the peaks of them are greater than 99, which means that the conversion efficiency defined in Eq. (13) can go beyond 99% when the aperture angles of elliptical mirrors with different eccentricities are greater than π. It can, therefore, be concluded that elliptical mirror is a more effective focusing element to acquire strong and pure longitudinal field in the focal plane.

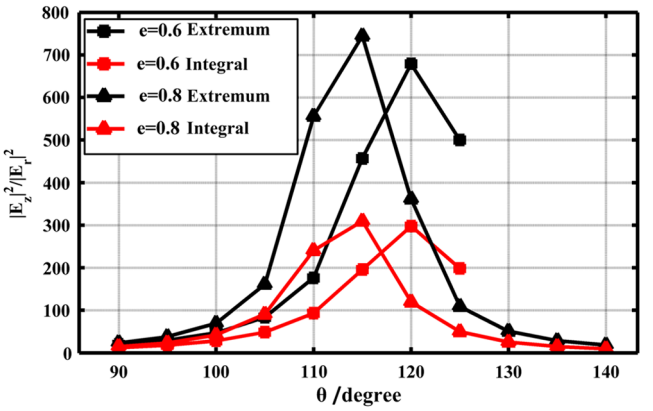

Fig. 9 Ratios of longitudinal and radial components of field intensity of elliptical mirrors for different eccentricities. Two components are compared by maximum and integral intensity in the focal plane, which are marked by data in black and red, respectively.

5 Conclusions

A concise analytic expression of apodization function was derived for an elliptical mirror. The focusing properties under linearly and radially polarized illuminations were studied using this apodization function when the aperture angle of the elliptical mirror is greater than π. It was found that a bone-shaped focal spot can be generated by focusing a linearly polarized beam and a tight-circularly symmetric spot can be formed by focusing a radially polarized one. The conversion efficiency of the longitudinal field in an EMBS can go beyond 99% under radially polarized illumination, which means that a quite strong and pure longitudinal field near the focal region can be obtained. The nature of an elliptical mirror with two conjugate foci makes it attractive for scanning microscopy, optical tweezers, and particle acceleration.

Acknowledgments

This work is funded by National Natural Science Foundation of China (Grant Nos. 50905048, 51275121, 51205089, and 61078049).

References

1. J. Liu et al., "Rigorous theory on elliptical mirror focusing for point scanning microscopy," *Opt. Express* **20**(6), 6175–6184 (2012).
2. J. Liu et al., "Elliptical mirror based imaging with aperture angle greater than $\pi/2$," *Opt. Express* **20**(17), 19206–19213 (2012).
3. L. Jian et al., "Focusing of cylindrical-vector beams in elliptical mirror based system with high numerical aperture." *Opt. Commun.* **305**, 71–75 (2013).
4. A. Drechsler et al., "Confocal microscopy with a high numerical aperture parabolic mirror," *Opt. Express* **9**(12), 637–644 (2001).
5. D. Zhang et al., "Parabolic mirror-assisted tip-enhanced spectroscopic imaging for non-transparent materials," *J. Raman Spectrosc.* **40**(10), 1371–1376 (2009).
6. T. Ruckstuhl and S. Seeger, "Confocal total-internal-reflection fluorescence microscopy with a high-aperture parabolic mirror lens," *Appl. Opt.* **42**(16), 3277–3283 (2003).

7. M. Lieb and A. Meixner, "A high numerical aperture parabolic mirror as imaging device for confocal microscopy," *Opt. Express* **8**(7), 458–474 (2001).
8. J. Stadler et al., "Tighter focusing with a parabolic mirror," *Opt. Lett.* **33**(7), 681–683 (2008).
9. E. Wolf, "Electromagnetic diffraction in optical systems. I. An integral representation of the image field," *Proc. R. Soc. A* **253**(1274), 349–357 (1959).
10. B. Richards and E. Wolf, "Electromagnetic diffraction in optical systems. II. Structure of the image field in an aplanatic system," *Proc. R. Soc. A* **253**(1274), 358–379 (1959).
11. M. Gu, *Advanced Optical Imaging Theory*, pp. 143–191, Springer, Berlin (1999).
12. Q. Zhan, "Cylindrical vector beams: from mathematical concepts to applications," *Adv. Opt. Photonics* **1**(1), 1–57 (2009).
13. H. Wang et al., "Creation of a needle of longitudinally polarized light in vacuum using binary optics," *Nat. Photonics* **2**(8), 501–505 (2008).
14. R. Dorn, S. Quabis, and G. Leuchs, "Sharper focus for a radially polarized light beam," *Phys. Rev. Lett.* **91**(23), 233901 (2003).
15. K. S. Youngworth and T. G. Brown, "Focusing of high numerical aperture cylindrical-vector beams," *Opt. Express* **7**(2), 77–87 (2000).
16. K. Huang et al., "Design of DOE for generating a needle of a strong longitudinally polarized field," *Opt. Lett.* **35**(7), 965–967 (2010).

Jian Liu obtained his BS degree from Southwest Jiaotong University, China, in 1997. He was then awarded the MS and PhD degrees from Harbin Institute of Technology in 2002 and 2009, respectively. In 2012, he became a professor in the Department of Automation Measurement and Control, Harbin Institute of Technology, China. His research interests include super-resolution light microscopy, precision measurement, and metrology.

Min Ai obtained his BS degree from Harbin Institute of Technology, China, in 2011. He is currently a second year MS student at Harbin Institute of Technology. His research interests are focusing theory and its related applications.

He Zhang obtained his BS degree from Harbin Institute of Technology, China, in 2012. He is currently a first year MS student at Harbin Institute of Technology, China. His research interests are focusing theory and its related applications.

Jiubin Tan received his BS, MS, and PhD degrees from the Department of Automation Measurement and Control, Harbin Institute of Technology, China, in 1982, 1988, and 1991, respectively. He became a professor of measurement and instrumentation in 1995 and was the dean of the Department of Automation Measurement and Control. He is currently the director of the Center of Ultra-precision Optoelectronic Instrument Engineering, Harbin Institute of Technology, China. His research covers a wide range of disciplines and technologies in the fields of ultra-precision measurement and instrumentation.